

Supporting Information

Tailored Nanoscale Structure of Flame-made Antimony Doped Tin Oxides and Their Near-Infrared Shielding Properties

Tung Van Pham,^a Tomoyuki Hirano,^{a} Eishi Tanabe,^a Eka Lutfi Septiani,^a Kiet Le Anh Cao,^a
and Takashi Ogi^a*

^a Chemical Engineering Program, Department of Advanced Science and Engineering,
Graduate School of Advanced Science and Engineering, Hiroshima University, 1-4-1
Kagamiyama, Higashi-Hiroshima City, Hiroshima 739-8527, Japan

^b Hiroshima Prefectural Institute of Industrial Science and Technology, 3-10-31 Kagamiyama,
Higashi-Hiroshima City, Hiroshima 739-0046, Japan

*Corresponding author:

Tomoyuki Hirano, tomoyuki-hirano@hiroshima-u.ac.jp

Tel/Fax: +81-82-424-3765

Section S1. Additional TEM and HRTEM images of flame-made ATO NPs.

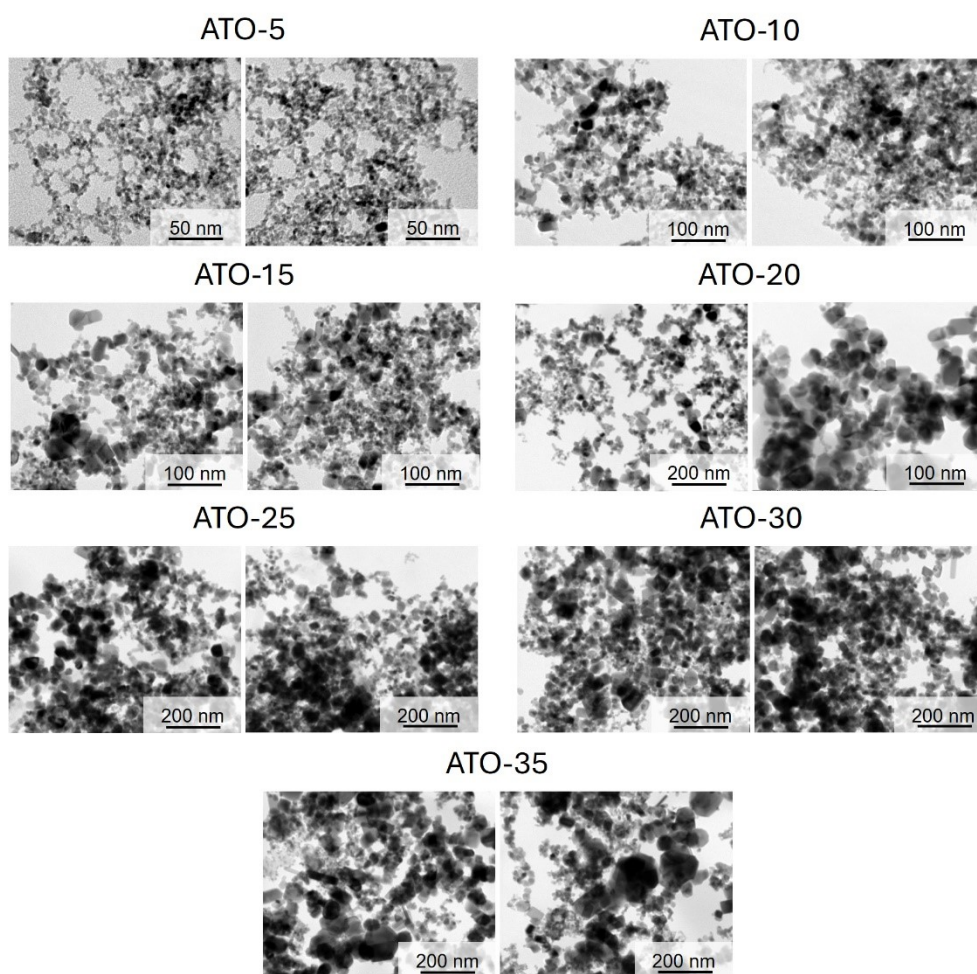


Figure S1. TEM images of various sized ATO NPs by FSP method (ATO-5 to ATO-35).

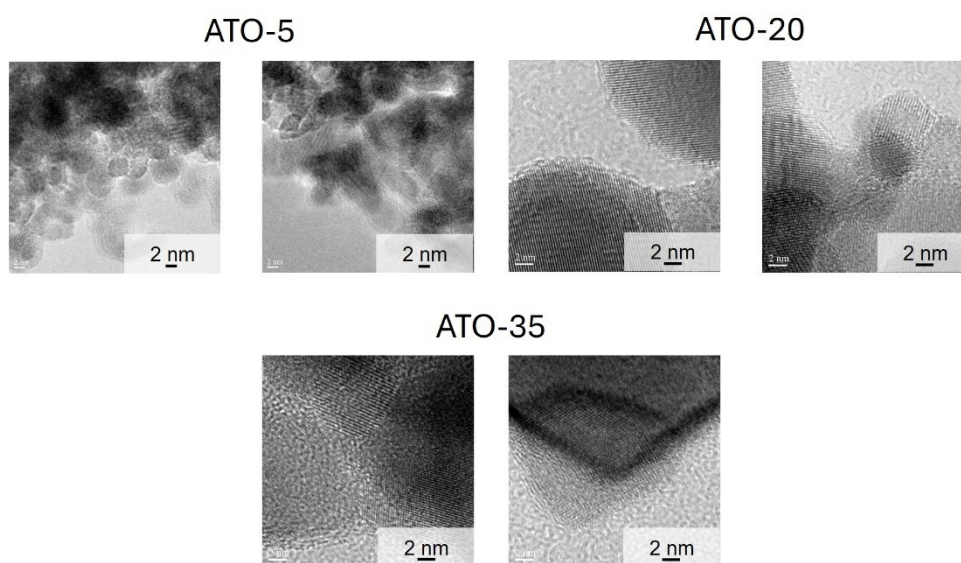


Figure S2. HRTEM images of various sized ATO NPs (ATO-5, ATO-20, and ATO-35).

Section S2. N₂ adsorption–desorption measurement and calculation for average BET particle diameter – d_{BET} of various sized ATO NPs.

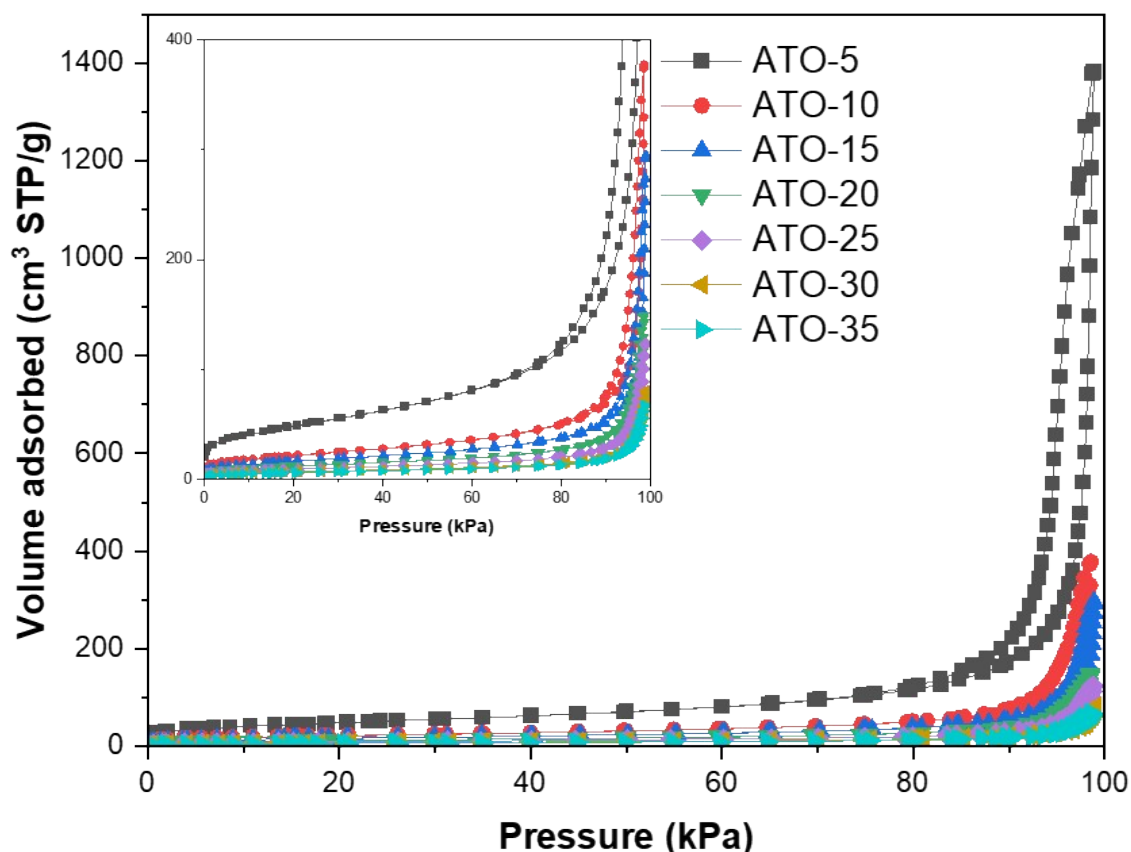


Figure S3. N₂ adsorption–desorption isotherm curves of the ATO NPs with various crystal size (5 – 35 nm).

Assuming that the particles are spherical and unaffected by aggregation or sintering during synthesis, the average BET particle diameter can be calculated using the following equation:

$$d_{BET} = \frac{6 \times 1000}{SSA \times \rho} \quad (1)$$

where d_{BET} represents the average BET particle diameter (in nm), SSA denotes the specific surface area (in m²/g) of the particles, as determined by nitrogen adsorption–desorption

measurements at 77 K using a BELSORP-max instrument and the BET method, and ρ is the density of tin oxide (6.95 g/cm³). The contribution of antimony doping is neglected in this calculation for simplicity. The results of the calculation are presented in **Table S1**.

Table S1. The detailed calculation results of the average BET particle diameter, along with the comparison between the BET diameter, crystal size, and particle size.

Sample	SSA (m ² /g)	Average BET particle diameter – d_{BET} (nm)	Crystal size – d_c (nm)	Particle size – d_p (nm)	The different between d_{BET} and d_c (%)	The different between d_p and d_c (%)
ATO-5	173.00	4.99	4.80	5.1	4.0	6.3
ATO-10	79.30	10.89	9.70	10.1	12.3	4.1
ATO-15	59.62	14.48	15.71	15.1	-7.8	-3.9
ATO-20	42.02	20.54	20.26	19.3	1.4	-4.7
ATO-25	32.86	26.27	25.21	25.4	4.2	0.8
ATO-30	28.59	30.19	29.52	30.0	2.3	1.6
ATO-35	24.02	35.94	34.51	34.1	4.1	-1.2

Section S3. Flame condition for synthesizing ATO NPs and calculation for combustion enthalpy density.

Table S2. The detailed condition of flame and precursor for synthesizing ATO NPs with various crystal sizes.

Sample	Flame condition			Precursor condition	
	Air flow rate (L/min)	CH ₄ flow rate (L/min)	O ₂ flow rate (L/min)	Feed flow rate (mL/min)	Precursor total concentration (M)
ATO-5	3.67	1.55	5	1.5	0.1
ATO-10	3.67	1.55	3	3	0.1
ATO-15	3.67	1.55	3	4	0.5
ATO-20	3.67	1.55	3	5	0.5
ATO-25	3.67	1.55	3	7	1.2
ATO-30	3.67	1.55	3	15	1
ATO-35	3.67	1.55	3	25	1.2

The combustion enthalpy density was identified as the ratio of the fed liquid precursor combustion enthalpy (kJ/min) over the total gas flow (g_{gas}/min). The combustion enthalpy density for each synthesis condition of prepared ATO NPs is calculated based on the equation below.

$$\Delta h_{combustion} = \frac{-\dot{n}_{xylene} \times \Delta H^0_{combustion, Xylene}}{(\dot{m}_{gas})} = \frac{\Delta \dot{H}_{combustion, Xylene}}{(\dot{m}_{gas})} \quad (2)$$

Where $\Delta h_{combustion}$ represents for specific combustion density (kJ/g), and \dot{n}_{xylene} , denotes the molar flow rate of xylene (mol/min). $\Delta H^0_{combustion, Xylene}$ is the standard combustion enthalpy of xylene, which is -4552.9 kJ/mol, and $\Delta \dot{H}_{combustion, Xylene}$ refers to the combustion enthalpy of xylene (kJ/min) at the given molar flow rate (\dot{n}_{xylene}).

Additionally, the mass flow rate of the gas mixture (\dot{m}_{gas}) is calculated using the following equation:

$$\dot{m}_{gas} = \dot{m}_{flame\ gas} + \dot{m}_{precursor\ evaporating} = Q_{O_2} \times \rho_{O_2} + Q_{CH_4} \times \rho_{CH_4} + Q_{Air} \times \rho_{Air} + Q_{precursor} \times \rho_{precursor} \quad (3)$$

Where Q_{CO_2} , Q_{CH_4} , Q_{Air} and $Q_{precursor}$ represent the volumetric flow rates (in mL/min or L/min) of oxygen as the dispersing gas, methane/air as the premixed flame, and the precursor, respectively. Detailed calculations are presented in **Table S3**.

Table S3. The detailed calculation of combustion enthalpy densities for synthesizing ATO NPs with various crystal sizes.

Sample	$\Delta \dot{H}_{combustion, Xylene}$ (kJ/min)	$\dot{m}_{flame\ gas}$ (g/min)	$\dot{m}_{precursor}$ (g/min)	Combustion enthalpy density (kJ/g _{gas})
ATO-5	53.52	16.78	1.31	2.96

ATO-10	107.05	13.93	2.62	6.47
ATO-15	123.62	13.93	3.74	6.99
ATO-20	154.53	13.93	4.68	8.30
ATO-25	157.82	13.93	7.30	7.43
ATO-30	374.02	13.93	15.18	12.85
ATO-35	563.66	13.93	26.07	14.09

Section S4. Hydrodynamic particle size of flame-made ATO NPs by DLS measurement.

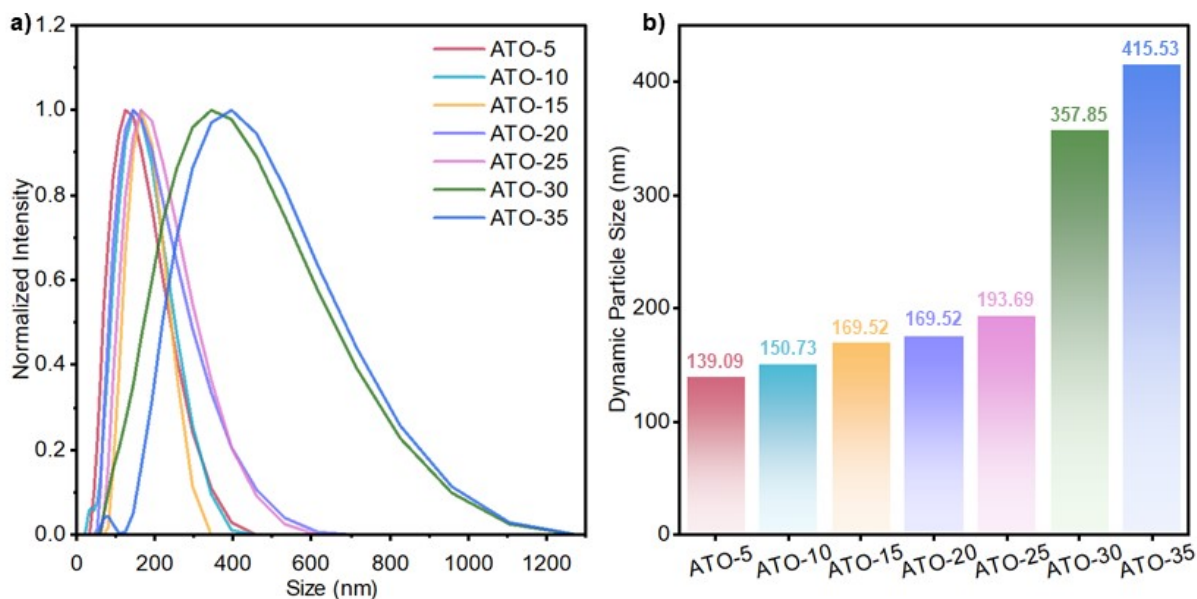


Figure S4. Particle size distribution of various sized ATO NPs by DLS measurement and their average hydrodynamic diameters.

While **ATO-5** to **ATO-25** exhibit a gradual increase in hydrodynamic diameter, a notable jump is observed for **ATO-30** (357.85 nm) and **ATO-35** (415.53 nm), suggesting significant agglomeration in these samples. This deviation from the trend can be attributed to enhanced interparticle interactions, as larger particles inherently possess lower specific surface areas and stronger van der Waals forces, which facilitate clustering in dispersion. In addition, to promote crystal growth in the synthesis of larger ATO NPs, the feed flow rate was significantly increased for **ATO-30** and **ATO-35**. While this adjustment provides additional thermal energy necessary for crystal growth, it also intensifies agglomeration processes during flame synthesis. The increased energy leads to higher particle collision frequencies and promotes the formation of soft agglomerates, which are not fully broken apart during dispersion. Consequently, this combination of physical and processing factors contributes directly to the sharp increase in hydrodynamic diameters observed for **ATO-30** and **ATO-35** in the DLS measurements.

Section S5. Wide-scan XPS spectra of as-synthesized ATO NPs.

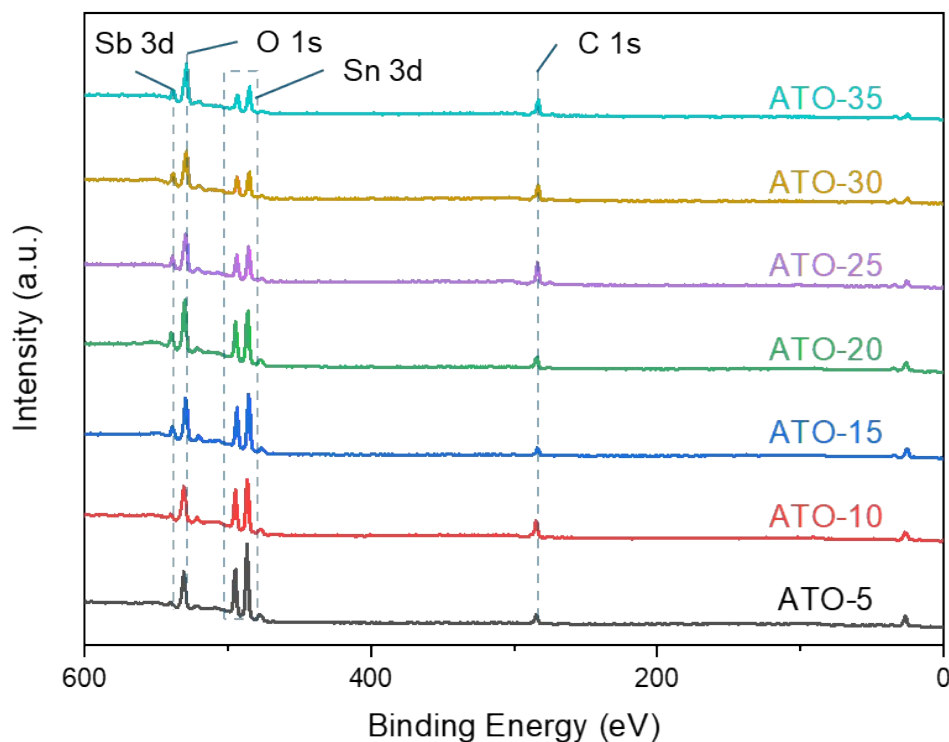


Figure S5. Wide-scan XPS spectra of as-synthesized ATO NPs (ATO-5 to ATO-35), highlighting the presence of Sn, Sb, O, and C.

Section S6. Calculation for equivalence ratios of each flame condition of synthesizing various-sized ATO NPs.

To explain the phenomenon where the proportion of Sb^{3+} ions increase with the crystal size of ATO nanoparticles (NPs), equivalence ratios were calculated to determine whether the synthesis conditions were fuel-lean or fuel-rich. The calculation of the equivalence ratios is based on the following equation:

$$\Phi = \frac{AFR (stoich)}{AFR (act)} \quad (4)$$

Where Φ represents the equivalence ratio of combustion reactions of xylene during the synthesis of ATO nanoparticles. A $\Phi = 1$ corresponds to a stoichiometric ratio, $\Phi > 1$ indicates

a fuel-rich condition leading to a lack of oxidative environment and unburned fuel, and $\Phi < 1$ signifies a fuel-lean condition, meaning the fuel has been completely combusted in an oxidative environment. The *AFR (act)* is the ratio of the mass of air to the mass of fuel (xylene) used in each experimental condition. The *AFR (stoich)* is the theoretical ratio between the mass of air and the mass of fuel, calculated based on the complete combustion reaction of xylene in air, as determined by the following equation:



$$AFR (stoich) = \frac{m_{air, stoich}}{m_{fuel, stoich}} = \frac{10.5 \times \frac{100}{21} \times 28.96}{1 \times 106.16} = 13.64 \left(\frac{g_{air}}{g_{fuel}} \right) \quad (6)$$

Table S4. The detailed calculation of equivalence ratios for each flame condition of ATO NPs.

Sample	$M_{air, act}$ (g_{air})	$M_{fuel, act}$ (g_{fuel})	AFR, act (g_{fuel})	Φ (-)	Fuel state (-)
ATO-5	39.40	1.27	30.99	0.44	Fuel lean
ATO-10	27.09	2.54	10.65	1.28	Fuel rich
ATO-15	27.09	2.93	9.22	1.48	Fuel rich
ATO-20	27.09	3.67	7.38	1.85	Fuel rich
ATO-25	27.09	3.75	7.22	1.89	Fuel rich
ATO-30	27.09	8.88	3.04	4.49	Fuel rich
ATO-35	27.09	13.39	2.02	6.75	Fuel rich

Section S7. Normalized representation, 3D visualization of UV–VIS–NIR spectra and optical band gap calculation using the Tauc plot method for flame-made ATO NPs (5–35 nm).

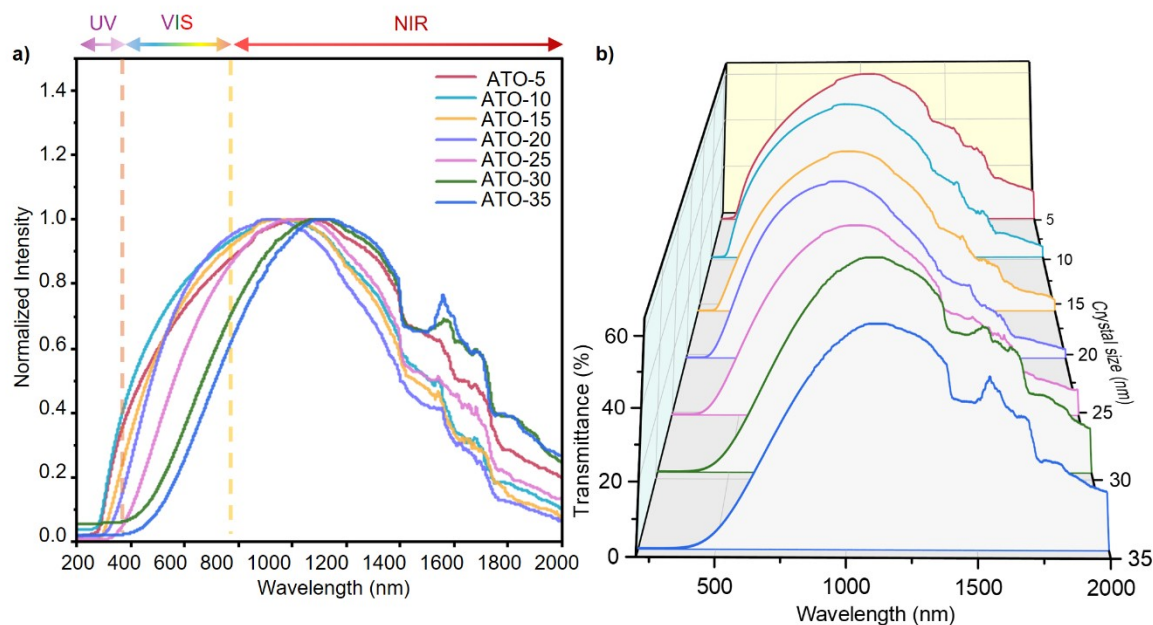


Figure S6. (a) Normalized representation and (b) 3D visualization of UV–VIS–NIR spectra of flame-made ATO NPs with various crystal/particle diameters (around 5–35 nm).

Table S5. Average transmittances in ultraviolet wavelength range (T_{UV} , 200–380 nm) visible wavelength range (T_{VIS} , 380–780 nm), and near–infrared wavelength range (T_{NIR} , 780–2000 nm) of prepared ATO-NPs with various sizes.

Sample	$T_{UV, 200-380 \text{ nm}}$ (%)	$T_{VIS, 380-780 \text{ nm}}$ (%)	$T_{NIR, 780-2000 \text{ nm}}$ (%)
ATO-5	7.34	41.76	42.26
ATO-10	7.69	45.65	36.30
ATO-15	3.90	40.28	34.66
ATO-20	1.93	41.32	33.61
ATO-25	0.55	31.07	38.14
ATO-30	0.08	19.33	44.77
ATO-35	0.05	15.09	43.36

From the obtained UV–VIS–NIR spectra, the Tauc plot method was employed to calculate the band gap energy of ATO NPs with varying sizes, providing insight into the changes in the electrical properties of the as-synthesized samples.

The UV–VIS–NIR transmittance spectra of ATO NPs dispersed in ethanol were converted to absorbance using **Equation 7**. The absorption coefficient (α) was then determined using **Equation 8**, where A represents absorbance and L is the cuvette path length (1 cm). The Tauc plot equation (**Equation 9**) was constructed by plotting $(\alpha h\nu)^{(1/r)}$ against photon energy ($h\nu$), where $h\nu = 1240/\lambda$ (λ in nm) and K represent for energy dependent constant. The analysis was conducted assuming a direct band gap transition ($r = 1/2$). The band gap energy was obtained by extrapolating the linear region of the plot to the x-axis. Table S6 provides a summary of the linear plots and the calculated band gap values of the as-synthesized ATO NPs.

$$A = -\log_{10}(T) \quad (7)$$

$$\alpha = \frac{(2.303 \times A)}{L} \quad (8)$$

$$(\alpha h\nu)^2 = K(h\nu - E_g) \quad (9)$$

Table S6. Detailed calculations of band gap energy of various size ATO NPs with Tauc plot method.

Sample	$y = a + bx$			Band gap energy – E_g (eV)
	a	b	R^2	
ATO-5	-4311.82	1046.61	0.99	4.11
ATO-10	-5944.69	1447.94	0.99	4.11
ATO-15	-8808.37	2165.76	0.99	4.07
ATO-20	-9230.61	2386.46	0.99	3.87
ATO-25	-10592.68	2794.27	0.99	3.71
ATO-30	-11402.1	3115.37	0.99	3.66
ATO-35	-11510.38	3137.16	0.99	3.67

